
**STRENGTH
AND PLASTICITY**

Prediction of the Hot flow Behavior of AA1070 Aluminum Using the Phenomenological and Physically-Based Models

H. R. Rezaei Ashtiani^{a, *, **} and A. A. Shayanpoor^a

^a *School of Mechanical Engineering, Arak University of Technology, Arak, 38135-1177, Iran*

^{*}*e-mail: hr_rezaei@arakut.ac.ir*

^{**}*e-mail: hrr.Ashtiani@gmail.com*

Received January 6, 2021; accepted March 8, 2021

Abstract—For the prediction of the hot flow behavior of materials, the constitutive models have developed in a form that feeds in computer code to simulate the response of workpiece under the process loading conditions. For this purpose, the hot compression tests were used at different ranges of temperature (623–773 K) and strain rate (0.005–0.5 s⁻¹) for AA1070 aluminum. In this study constitutive equations based on the modified Johnson–Cook (JC) and modified Zerilli–Armstrong (ZA) models were established using the experimental data and were compared with an earlier study for the strain-compensated Arrhenius (strain-com Arr) model to predict the hot flow behavior of the pure aluminum. Then terms of the correlation coefficient (*R*), relative error (RE), and average absolute relative error (AARE) were used to evaluate the comparative predictability of these models. The *R* values for the modified J–C and modified Z–A are 0.9759 and 0.9760, respectively. Also, The AARE and mean RE values obtained for the modified J–C model are 9.085 and 1.6624% and for modified Z–A are 7.901 and 0.7840%, respectively.

Keywords: hot deformation behavior, constitutive model, AA1070 aluminum, phenomenological model, physically-based model

DOI: 10.1134/S0031918X21130160

1. INTRODUCTION

The appropriate properties consist of good fracture toughness, high strength to weight ratio and corrosion resistance of aluminum alloys made widely used in various industries such as aircraft, packaging, automobile, etc. [1, 2].

The flow behaviors of materials are very complex at high temperatures so the prediction of this behavior is difficult and complicated and to develop and establish the proper constitutive equations is very important. As one of the necessary processes in the manufacturing of engineering, hot forming is an essential step to control the microstructure and performance. The hardening and softening mechanisms are affected by processing parameters such as the amount of deformation, deformation temperature, and rate. One of the most essential performance indexes for the hot forming process is material flow behavior that are significant reactions of work-hardening, work-softening, dynamic recovery (DRV), and dynamic recrystallization (DRX) process [3].

For modeling the response of workpiece at different loading conditions, material flow behaviors must feed in computer code using the proper constitutive [4]. The accuracy of the developed constitutive equa-

tion generally determines the accuracy of the simulated results.

The investigations of material hot flow behavior showed that the empirical, semi-empirical, phenomenological, physically-based models as constitutive models and artificial neural networks (ANN) model have been constructed to predict the flow behavior at different temperatures (*T*), strain (ϵ), and strain rates ($\dot{\epsilon}$) [5–7]. Phenomenological models are developed based on experimental observation using mechanical tests as the material constants of developed equations are obtained from fitting the experimental data and there are no physical characteristics that are taking into consideration. The Johnson–Cook (J–C) [8], Khan–Huang–Liang (K–H–L) [9], and Arrhenius-type [10] models are examples of phenomenological constitutive models which are extensively used to predict the hot flow behavior of materials as *T*, ϵ , and $\dot{\epsilon}$ dependent models. Rezaei Ashtiani et al. [11] developed a constitutive equation that considers strain and investigated the influence of initial grain size on hot working behavior for the commercial purity aluminum. Cai et al. [12] established a suitable modified J–C constitutive model for Ti–6Al–4V alloy in different values of *T* and $\dot{\epsilon}$. Meanwhile, the deformation mechanism as the internal microstructure changing

during deformation, including dislocation mechanisms, thermodynamics theory and slips kinetics the physically-based model usually considers, especially in relatively high T and $\dot{\epsilon}$ conditions. Li et al. [13] investigated the phenomenological Arrhenius-type constitutive model of the hot flow behavior in AA6082 aluminum alloy and they reported this model was more efficient for tracking the flow of this alloy.

Zerilli–Armstrong (Z–A) model [14] is one of the physical models can be characterized by flow stress behavior at elevated temperature. Zhang et al. [15] developed a modified Z–A constitutive equation by considering the effects of T , $\dot{\epsilon}$, and deforming process on certain parameters and accurately describe the high-temperature flow stress of IC10 alloy by a tensile test over a wide range of T and $\dot{\epsilon}$. The constitutive relation of a new high-strength low-alloy steel with modified Z–A was investigated by Venkata Ramana et al. [16]. Ahmadi et al. [17] investigated a study on the phenomenological, physically-based, and ANN models to predict the hot flow stress of API 5CT-L80 steel. They showed that the three developed models have good accuracy to predict behavior of this steel at elevated temperatures.

In this paper, the influences of forming parameters such as ϵ , T , and $\dot{\epsilon}$ values on the flow stress of AA1070 aluminum are investigated by isothermal hot compressive tests. The main objective of this study is to derive constitutive equations relating to flow stress, T and $\dot{\epsilon}$ with modified J–C and modified Z–A to predict the flow behavior of AA1070 aluminum at high temperatures. Finally, the flow behavior predictions of these developed models were compared with the strain-compensated Arrhenius (strain-compensated Arr) model which were developed in the earlier study [4].

2. EXPERIMENTAL

The chemical composition of AA1070 aluminum employed in this study is given in Table 1. The aluminum was machined into cylindrical specimens with height and diameter of 12 and 8 mm, respectively, for hot compression test consenting to ASTM: E-209 standard. The uniaxial hot compression tests were applied by a Gotech-A17000 servo control electronic universal testing machine to determine the true stress-strain behavior of the alloy. Compression tests were carried out uniaxially up to the true strain of 0.6 and at different T of 623, 723, and 773 K and $\dot{\epsilon}$ of 0.005, 0.05, and 0.5 s^{-1} .

3. RESULTS AND DISCUSSION

3.1. Flow Stress Curves

The true stress–strain data taken from a hot compression test under the already mentioned experimental conditions of the AA1070 aluminum are plotted in

Table 1. Chemical composition (wt %) of AA1070 aluminum

Ti	Fe	Si	Zn	Ga	Cu	Al
0.0126	0.199	0.0778	0.0102	0.010	0.0102	99.7

Fig. 1 (tested by Rezaei Ashtiani et al. [4]). As it is clear, at the initial step of deformation, the flow stress enhances a quick rate due to work hardening where dislocation production, propagation, and trap occur.

After this increment when the flow stress attains the peak value, the work hardening rate reduces with increasing work softening therefore a steady-state is received or a slight increment up to final deformation

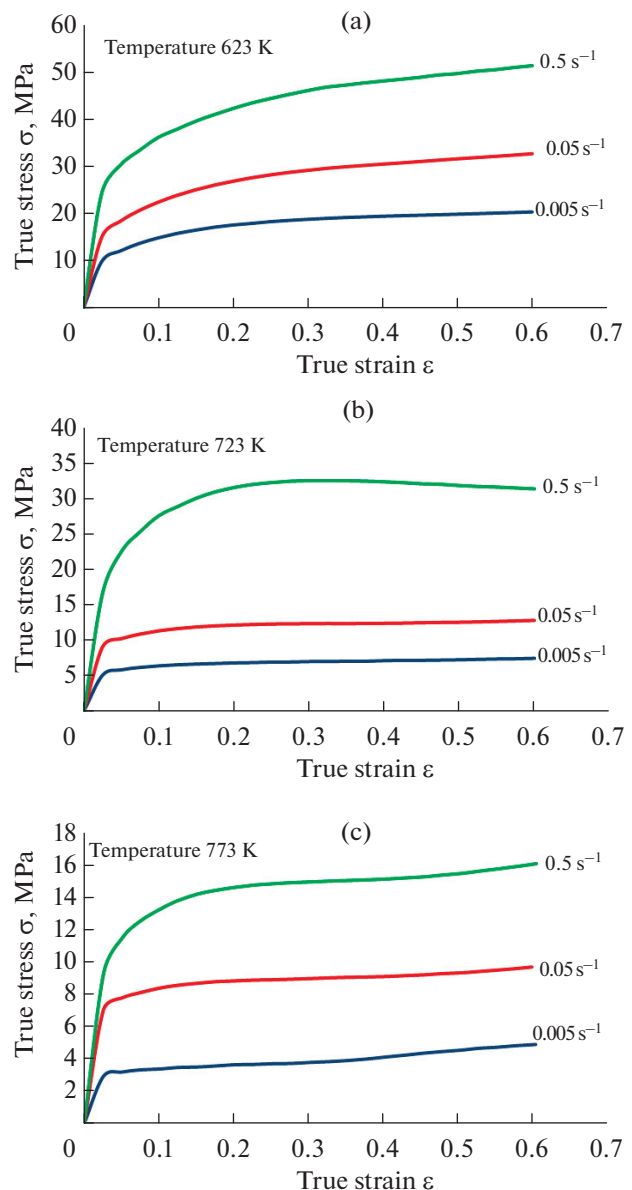


Fig. 1. The true strain–stress curves of the pure aluminum at various $\dot{\epsilon}$ and T of (a) 623, (b) 723, and (c) 773 K [4].

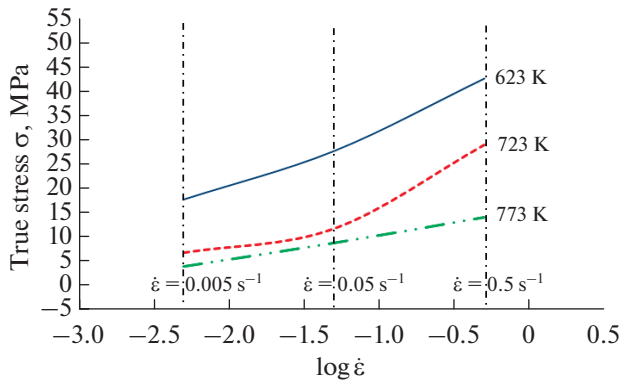


Fig. 2. Effects of $\dot{\epsilon}$ and T on the flow stress behavior of AA1070 aluminum.

at all process conditions, while hardening is dominated mechanism at T of 623 K. The attainment of steady-state values of flow values with increasing T to 773 K is a clear sign of thermal softening processes. As the dislocation production rate due to deformation becomes equal to the dislocation annihilation rate, so the dislocation rearrangement occurs and a steady-state is finally obtained by DRV [18]. In other words, the equilibrium between dynamic softening and work hardening occurs. The main mechanisms of DRV are dislocation movements in the cross-slip and climb modes as the main thermal softening mechanism very easily occur in aluminum alloys that have high stacking fault energy [19].

The effect of $\dot{\epsilon}$ and T on flow stress in the logarithm scale is shown in Fig. 2. When $\dot{\epsilon}$ is at a high level, there is no proper time for the dislocation response and nucleation of RX. The dislocation motion increases with an increasing thermal activation energy of the alloy with increasing T . As a result, the nucleation and growth rate of recrystallization can increase. So, the true stress enhances with increasing $\dot{\epsilon}$ and decreasing T [20, 21].

3.2. Development of Constitutive Models

3.2.1. Modified J–C model. A phenomenological equation which is successfully developed for different materials at different ranges of $\dot{\epsilon}$ and T is the J–C constitutive model. A type of modified J–C model can be expressed as Eq. (1) [22]:

$$\sigma = (A_1 + B_1\epsilon + B_2\epsilon^2)(1 + C_1 \ln \dot{\epsilon}^*) \times \exp[(\lambda_1 + \lambda_2 \ln \dot{\epsilon}^*)(T - T_{\text{ref}})], \quad (1)$$

where σ and ϵ present the flow stress and plastic strain, respectively. $A_1, B_1, B_2, C_1, \lambda_1, \lambda_2$ are material constants. $\dot{\epsilon}^* = \dot{\epsilon}/\dot{\epsilon}_0$ is dimensionless strain rate, where $\dot{\epsilon}$ and $\dot{\epsilon}_0$ are strain rate and reference strain rate, respectively. T and T_{ref} are the current absolute temperature and

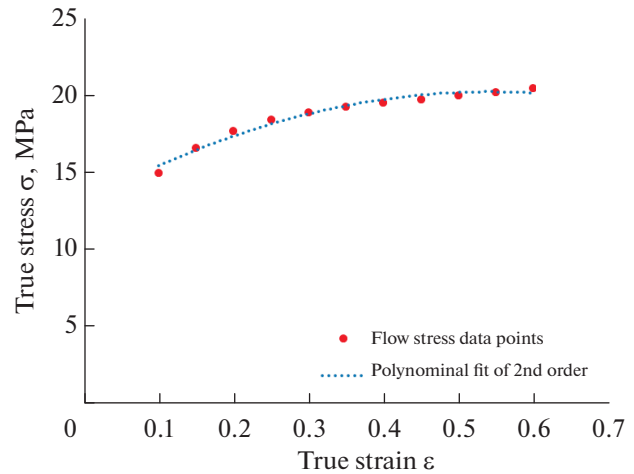


Fig. 3. Relationship between ϵ and σ at the T of 623 K and $\dot{\epsilon}$ of 0.005 s^{-1} .

reference temperature in Kelvin, respectively. In this study, the lowest experimental T and $\dot{\epsilon}$ conditions have been taken as reference temperature (T_{ref}) and reference strain rate ($\dot{\epsilon}_0$) which in the present case is 623 K and 0.005 s^{-1} , respectively. At reference condition, Eq. (1) can be rewritten as:

$$\sigma = (A_1 + B_1\epsilon + B_2\epsilon^2). \quad (2)$$

By substituting the experimental flow stress at the reference $\dot{\epsilon}$ and T , the curve between σ and ϵ can be gained as shown in Fig. 3. With the fitting of the second-order polynomial curve, the values of the constants of A_1, B_1 , and B_2 are obtained as 13.01, 26.767, and -24.697 MPa , respectively.

At reference T of 623 K Eq. (3) can be expressed as:

$$\frac{\sigma}{A_1 + B_1\epsilon + B_2\epsilon^2} = 1 + C_1 \ln \dot{\epsilon}^*. \quad (3)$$

The relation between $\sigma/(A_1 + B_1\epsilon + B_2\epsilon^2)$ and $\ln \dot{\epsilon}^*$ is obtained at different $\dot{\epsilon}$ as obvious in Fig. 4. The average slope of the linear fitting curve is used for evaluating C_1 value which in this state is 0.29998. At the final stage to establish the modified J–C model, a new parameter λ can be introduced by taking a natural logarithm on both sides to Eq. (1):

$$\ln \left(\frac{\sigma}{(A_1 + B_1\epsilon + B_2\epsilon^2)(1 + C_1 \ln \dot{\epsilon}^*)} \right) = \lambda(T - T_{\text{ref}}), \quad (4)$$

where $\lambda = \lambda_1 + \lambda_2 \ln \dot{\epsilon}^*$. The relation between $\ln(\sigma/(A_1 + B_1\epsilon + B_2\epsilon^2)(1 + C_1 \ln \dot{\epsilon}^*))$ and $(T - T_{\text{ref}})$ have been obtained as shown in Fig. 5 and the value of λ can be derived by the average slope of the plots. As shown in Fig. 6, the plot between $\ln \dot{\epsilon}^*$ and λ gives the

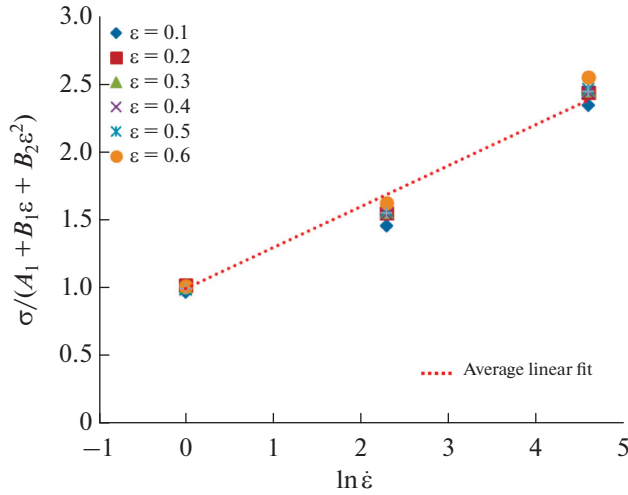


Fig. 4. Relationship between $\sigma / (A_1 + B_1\varepsilon + B_2\varepsilon^2)$ and $\ln \dot{\varepsilon}^*$ at different $\dot{\varepsilon}$ and T of 623 K.

value of $\lambda_1 = -0.0103$ as intercept and $\lambda_2 = 0.0009$ as slope, respectively. Consequently, after determining material constants, the constitutive model of pure aluminum based on the modified J–C equation can be gained.

3.2.2. Modified Z–A model. For the prediction of the hot flow behavior of materials, the modified Z–A model can be expressed as follows [23]:

$$\sigma = (C_1 + C_2\varepsilon^n) \exp[-(C_3 + C_4\varepsilon)T^* + (C_5 + C_6T^*) \ln \dot{\varepsilon}^*], \quad (5)$$

where $C_1, C_2, C_3, C_4, C_5, C_6,$ and n are material constants, ε is the plastic strain, $T^* = T - T_{\text{ref}}$ which T and T_{ref} are the current and reference temperature, respectively. $\dot{\varepsilon}^* = \dot{\varepsilon} / \dot{\varepsilon}_0$ is dimensionless strain rate, where $\dot{\varepsilon}$ and $\dot{\varepsilon}_0$ are strain rate and reference strain rate, respectively. Similar to the modified J–C model $\dot{\varepsilon}_0 = 0.005 \text{ s}^{-1}$ and $T_{\text{ref}} = 623 \text{ K}$ taken for reference strain rate and reference temperature, respectively. With taking natural logarithm on both sides of Eq. (5) can be obtained as follows at reference strain rate:

$$\ln \sigma = \ln (C_1 + C_2\varepsilon^n) - (C_3 + C_4\varepsilon)T^*. \quad (6)$$

The value of $\ln (C_1 + C_2\varepsilon^n)$ and $-(C_3 + C_4\varepsilon)T^*$ can be obtained from the intercept I_1 and the slope S_1 after performing linear fitting of the $\ln \sigma - T^*$ line, as shown in Fig. 7a.

$$I_1 = \ln (C_1 + C_2\varepsilon^n), \quad (7)$$

$$S_1 = (C_3 + C_4\varepsilon). \quad (8)$$

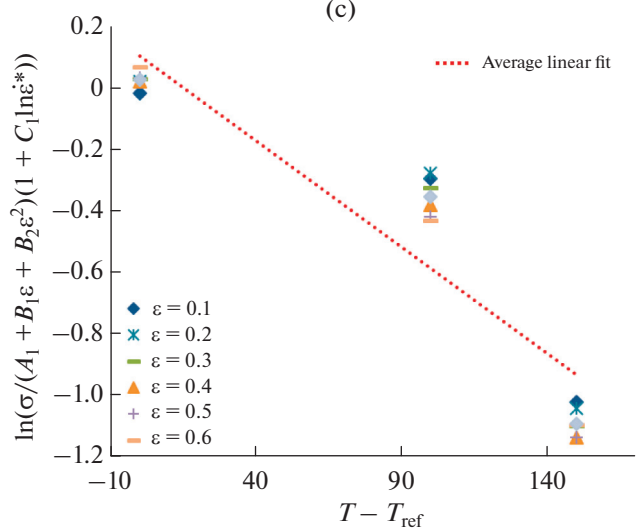
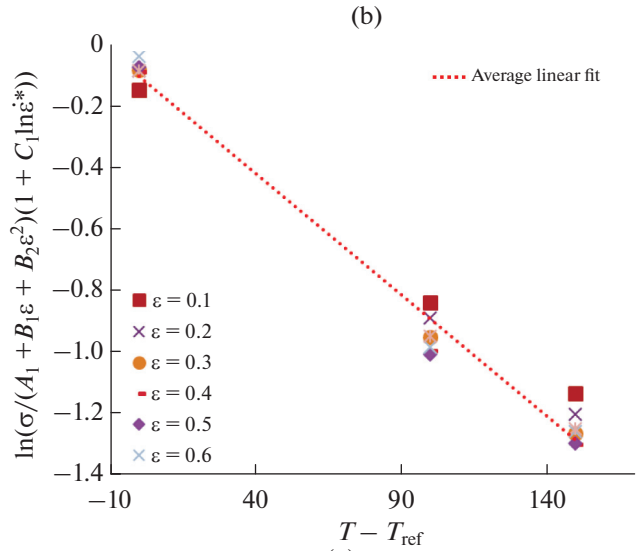
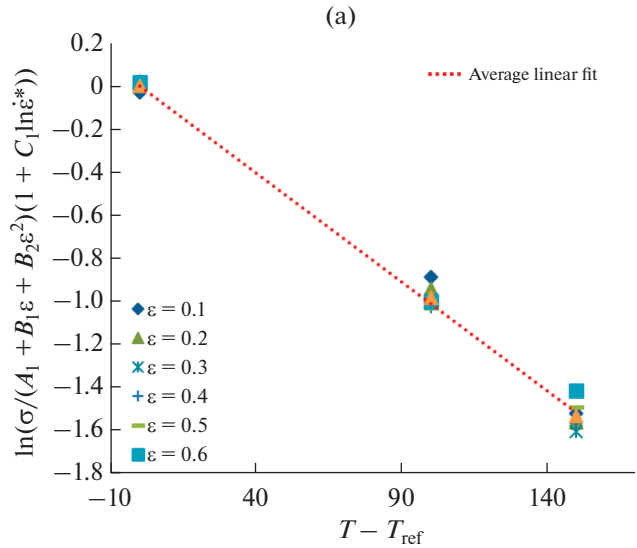


Fig. 5. Relationship between $\ln(\sigma / (A_1 + B_1\varepsilon + B_2\varepsilon^2) \times (1 + C_1 \ln \dot{\varepsilon}^*))$ and $(T - T_{\text{ref}})$ for $\dot{\varepsilon}$ of (a) 0.005, (b) 0.05, and (c) 0.5 s^{-1} .

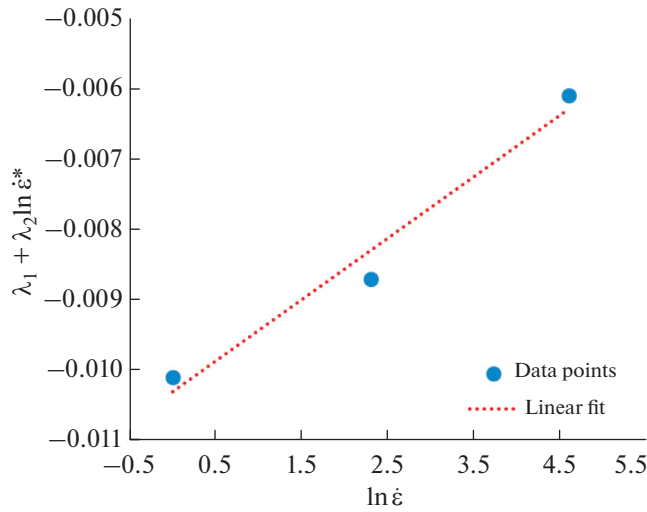


Fig. 6. Relationship between $\ln \dot{\epsilon}^*$ and $\lambda_1 + \lambda_2 \ln \dot{\epsilon}^*$.

Rearranging and taking a natural logarithm on both sides of Eq. (7), the following equation can be obtained.

$$\ln(\exp I_1 - C_1) = \ln C_2 + n \ln \epsilon, \quad (9)$$

where C_1 is evaluated as the flow stress of the material at reference conditions, which can be concluded from the experimental data. The relationship between $\ln \epsilon \sim \ln(\exp I_1 - C_1)$ is constructed as clear in Fig. 7b with substituting the value of C_1 in Eq. (9). The linear fit of the data points gives the values of the slope as n and intercept as C_2 , respectively. Similarly, the value of the slope C_3 and intercept C_4 can be calculated from S_1 versus ϵ plot according to Eq. (8), as shown in Fig. 7c. Another formation of Eq. (5) after taking natural logarithm can be written as follows:

$$\ln \sigma = \ln(C_1 + C_2 \epsilon^n) - (C_3 + C_4 \epsilon) T^* + S_2 \ln \dot{\epsilon}^*, \quad (10)$$

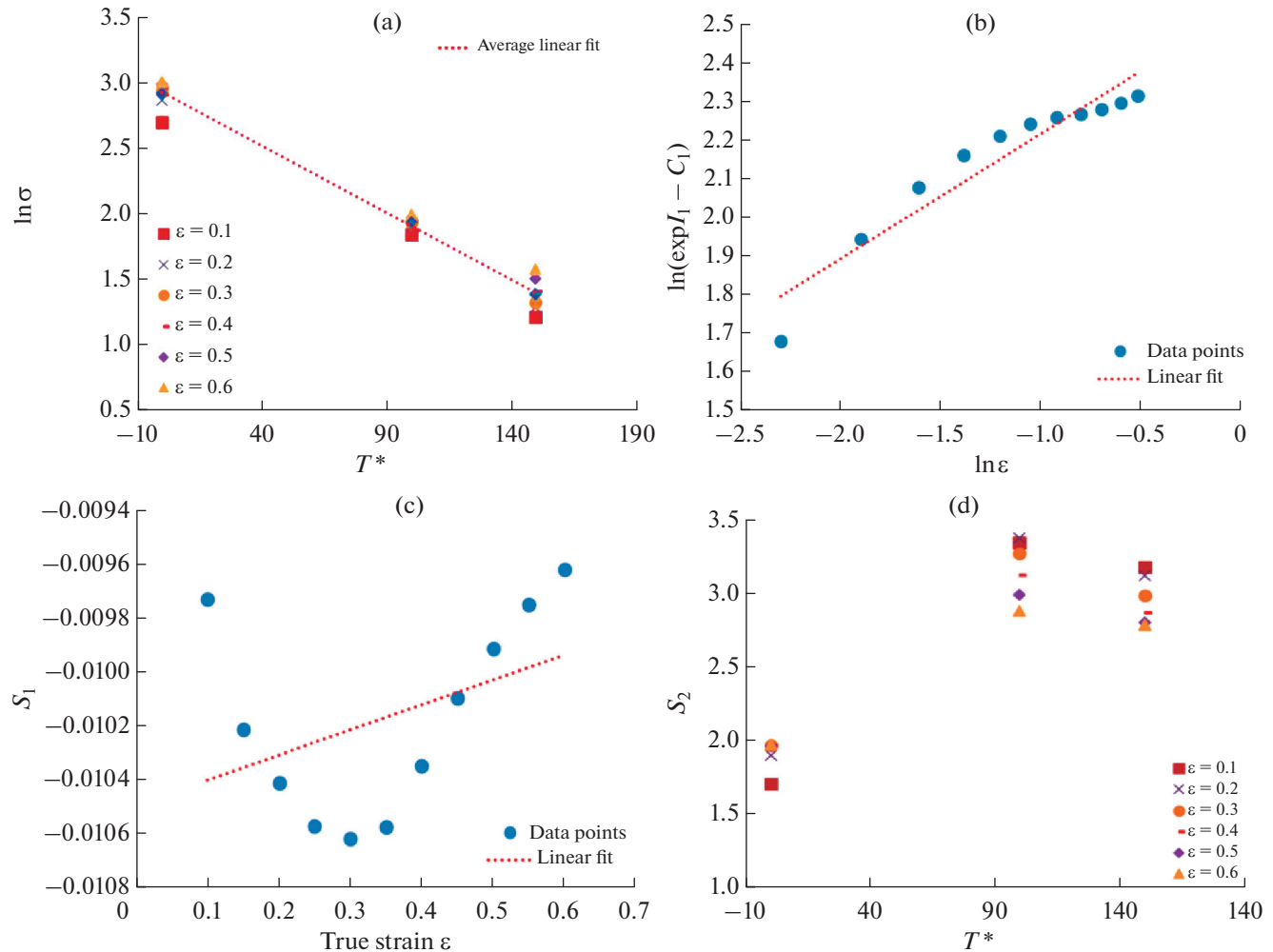


Fig. 7. (a) Relationship between T^* and $\ln \sigma$, (b) relationship between $\ln \epsilon$ and $\ln(\exp I_1 - C_1)$, (c) relationship between true strain (ϵ) and slope S_1 , and (d) relationship between T^* and slope S_2 .

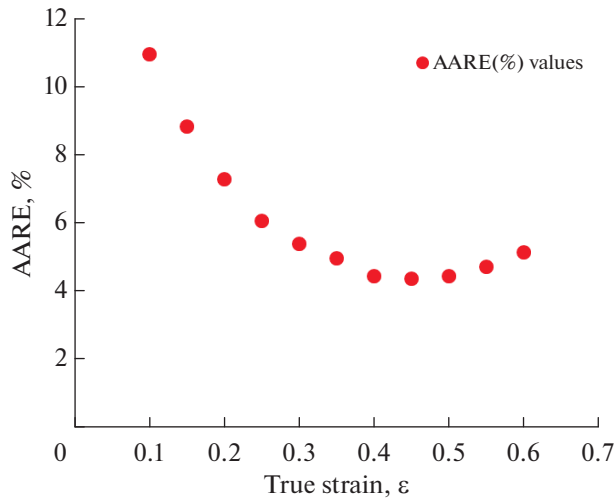


Fig. 8. Values of AARE percentage derived using different groups of C_5 and C_6 at eleven different strains.

where $S_2 = C_5 + C_6 T^*$. The relationship between $\ln \sigma$ and $\ln \dot{\epsilon}^*$ gained the value of S_2 at the true strain. The value of C_5 and C_6 can be calculated by the relationship between S_2 and T^* as shown in Fig. 7d. Eleven sets of C_5 and C_6 are obtained at eleven different strains. To determine the optimum set of C_5 and C_6 values, a standard unbiased statistical parameter of average absolute relative error (AARE) is introduced as follows:

$$\text{AARE} = \left(\frac{1}{N} \right) \sum_{i=0}^N \left| \frac{E_i - P_i}{E_i} \right| \times 100, \% \quad (11)$$

P_i and E_i are predicted stress results obtained from equations and experimental data, respectively, and N is the total number of data employed in this investigation. The optimization is performed by minimizing the AARE value between experimental data and predicted flow stress. As it is clear in Fig. 8, the minimum value of AARE is obtained at a true strain of 0.45, and the corresponding value of C_5 and C_6 is 0.207 and 0.00064, respectively. Consequently, after predicting the material constants for the predicted flow stress, the constitutive equation based on the modified Z–A model can be taken.

3.3. Accuracy Analysis of the Developed Constitutive Equations

The constitutive models based on the modified J–C and modified Z–A have been established at different ϵ , $\dot{\epsilon}$, and T conditions. The comparisons between the experimental and predicted data of flow stress (using modified J–C and modified Z–A models) at various processing conditions have been shown in Figs. 9 and 10 respectively. It is clear that the predicted flow stress from the constitutive equations could follow the experimental data of pure aluminum

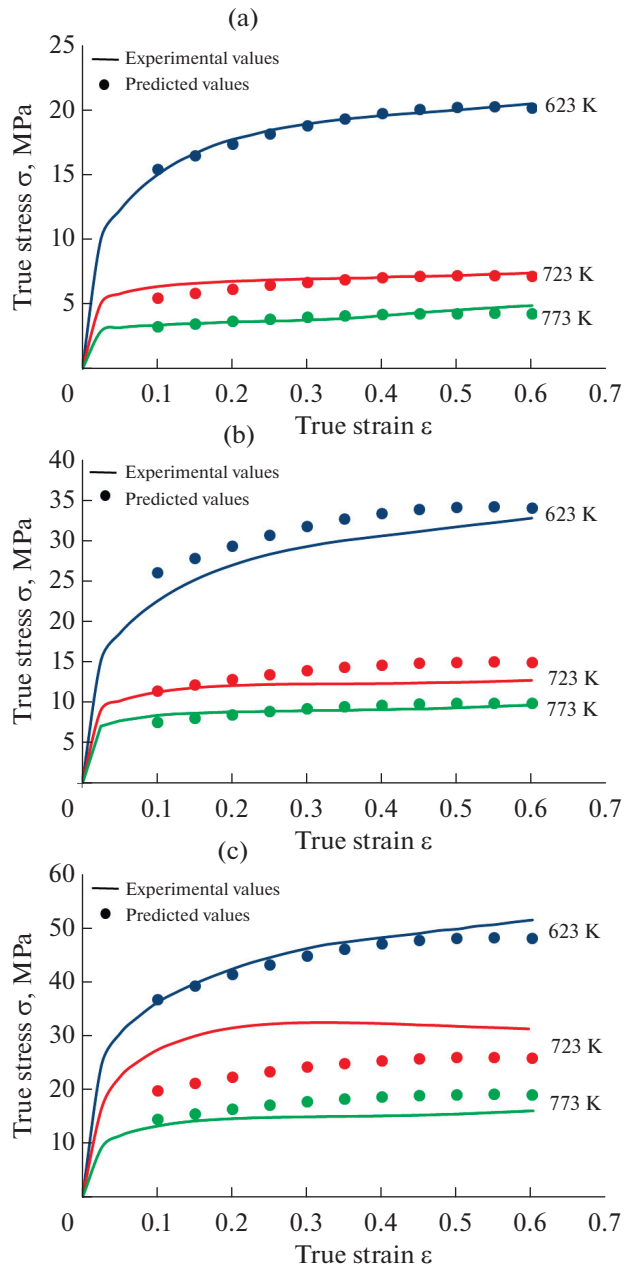


Fig. 9. Comparison between the experimental data and predicted data of flow stress by modified J–C model at various $\dot{\epsilon}$ and T of (a) 623, (b) 723, and (c) 773 K.

under most deformation conditions. The main reason for the deviation in physical and phenomenological with some experimental curves (i.e., in 0.5 s^{-1} at 723 K), may contribute to the fact that the flow behavior response of the materials at the elevated temperatures is highly nonlinear. Meantime, many factors that affect the flow stress are also nonlinear and probably because it is assumed that the material parameters are constants at various conditions, which decrease the validity of the predicted flow stress by the constitutive models and limit the practical range [12].

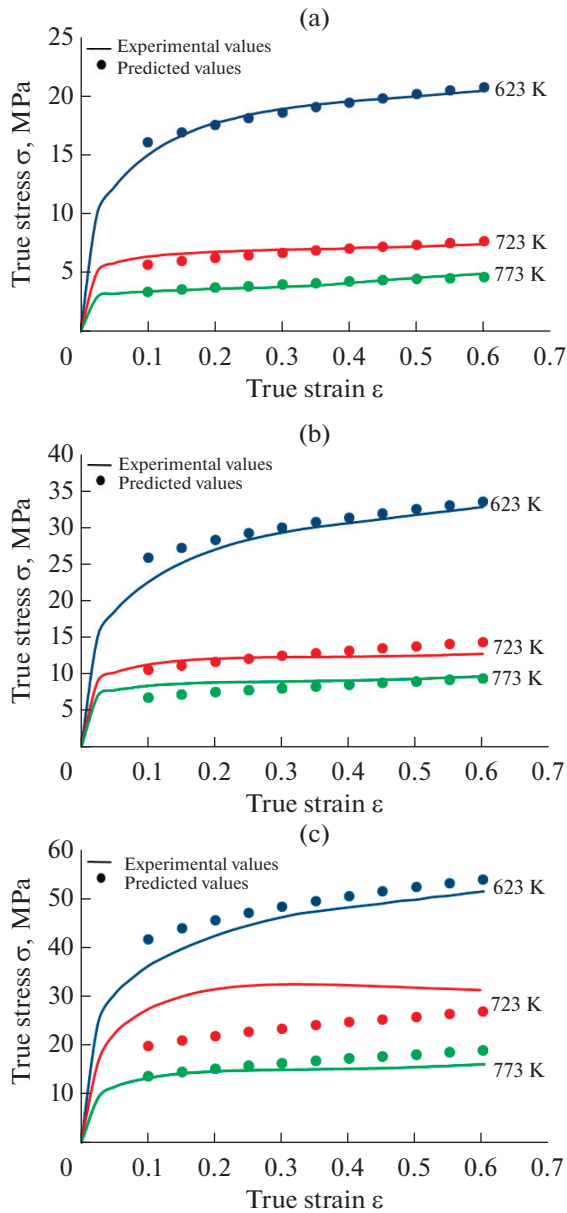


Fig. 10. Comparison between the experimental data and predicted data of flow stress by modified Z–A model at various $\dot{\epsilon}$ and T of (a) 623, (b) 723, and (c) 773 K.

The standard statistical parameters were employed in terms of correlation coefficient (R) and AARE, to assess the predictability of the constitutive models. R shows the linear relationship of predicted values and experimental data and can be expressed as:

$$R = \frac{\sum_{i=1}^N (E_i - \bar{E})(P_i - \bar{P})}{\sqrt{\sum_{i=1}^N (E_i - \bar{E})^2 \sum_{i=1}^N (P_i - \bar{P})^2}}, \quad (12)$$

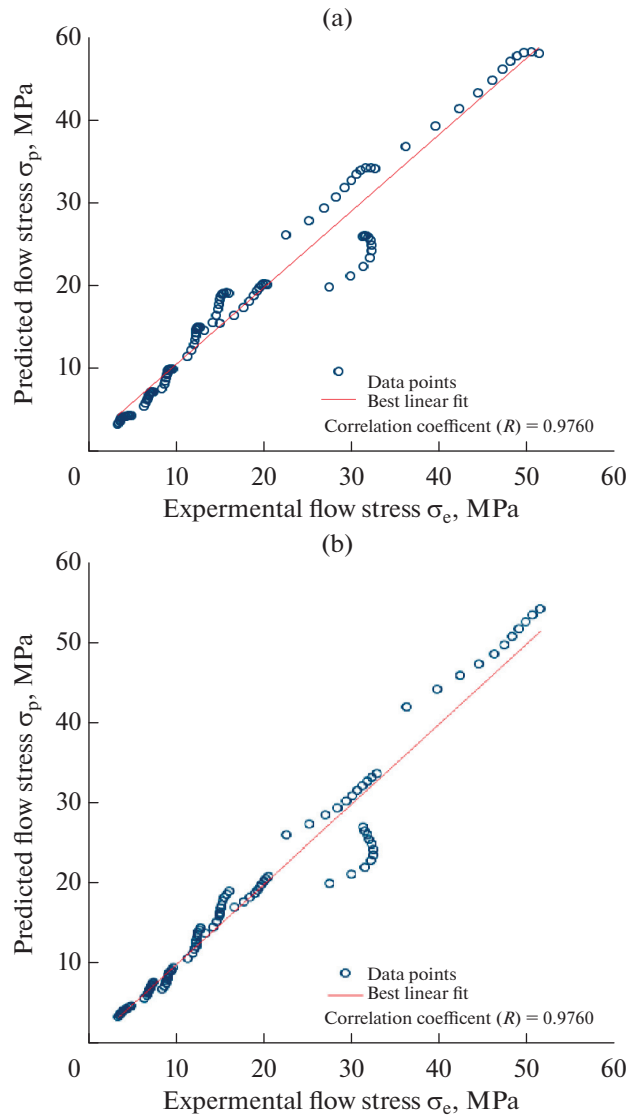


Fig. 11. Correlation between the experimental data and predicted data of flow stress values obtained from (a) modified J–C and (b) modified Z–A models.

where E_i and P_i have the same meaning as stated earlier. \bar{P} and \bar{E} are the mean values of predicted and experimental data, respectively, and N is the total number of data.

The correlations between experimental flow stress data and predicted values by modified J–C and modified Z–A models over the inter range of ϵ , $\dot{\epsilon}$, and T have been shown in Figs. 11a and 11b. It is obvious that the data points in different models lie nearby to the line.

The predictability of the developed models is studied by computing relative error percentage analysis.

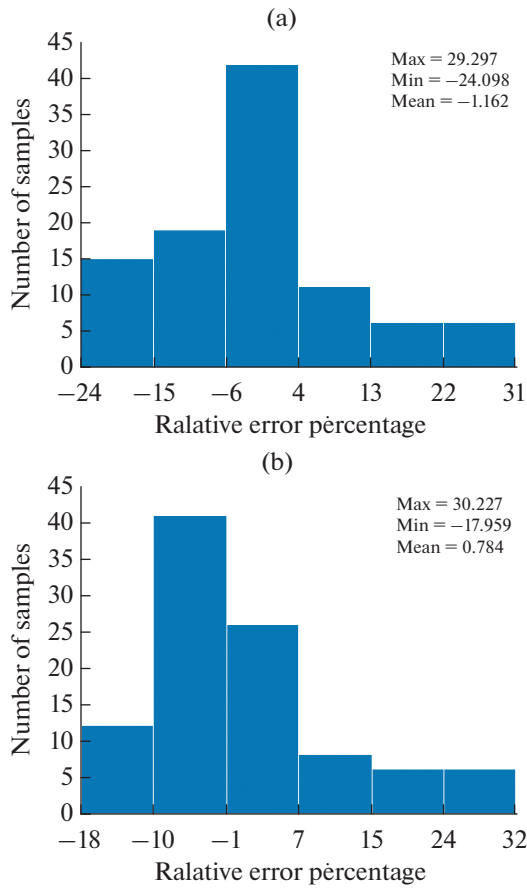


Fig. 12. Results of relative error analysis by (a) modified J-C and (b) modified Z-A models.

The formula of relative error (RE) can be expressed as follows:

$$\text{Relative error} = \left(\frac{E_i - P_i}{E_i} \right) \times 100, \% \quad (13)$$

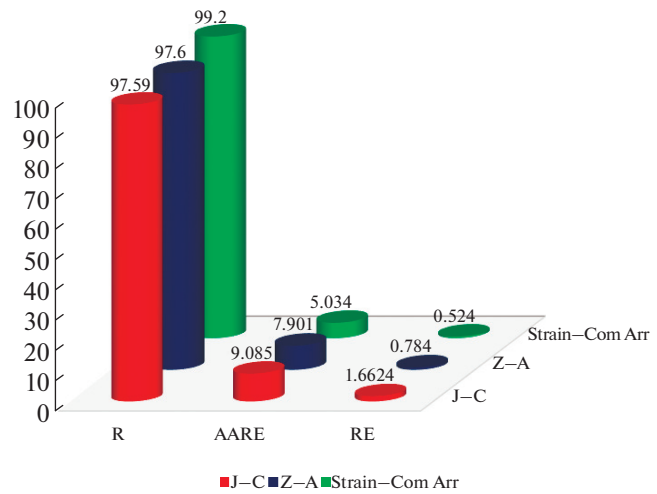


Fig. 13. Comparison in terms of statistical parameters between different developed constitutive models.

The meaning of E_i and P_i has mentioned earlier. The comparison of relative error between the experimental and predicted stress by the phenomenological and physical models are represented in Figs. 12a and 12b, respectively. The relative error variation for the modified JC model is -24.097 to 29.29% with a mean RE of 1.6624% and for the modified Z-A model it varies from -17.95 to 30.22% with a mean RE of 0.7840% and for the Strain-com Arr model [4] with mean RE of 0.5240%.

Comparatively, the different constitutive equations and related statistical parameters of AA1070 aluminum show in Table 2 and Fig. 13. It can be seen from this table that the R values of the modified J-C, modified Z-A, and Strain-com Arr models [4] are 0.9759, 0.9760, and 0.9920, respectively. Besides, The AARE value obtained for the modified J-C model is 9.085

Table 2. Comparison of various constitutive equations and statistical parameters for AA070 aluminum at the elevated deformation temperature

Models	Equation	R	AARE %	Mean RE%
M J-C	$\sigma = (13.01 + 26.767\epsilon - 24.697\epsilon^2) \times (1 + 0.29998 \ln \dot{\epsilon}^*) \times 1/2 \exp [(-0.0103 + 0.0009 \ln \dot{\epsilon}^*)(T - T_{ref})]$	0.9759	9.085	1.6624
M Z-A	$\sigma = (10.059 + 12.6923\epsilon^{0.3224}) \times \exp [-(0.0105 - 0.0009\epsilon)T^* + (0.207 + 0.00064T^*) \ln \dot{\epsilon}^*]$	0.9760	7.901	0.7840
Strain-com Arr model [4]	$\sigma = \frac{1}{\alpha} \ln \left\{ \left(\frac{Z}{A} \right)^{\frac{1}{n}} + \left[\left(\frac{Z}{A} \right)^{\frac{2}{n}} + 1 \right]^{\frac{1}{2}} \right\}$	0.9920	5.034	0.5240

and for modified Z–A is 7.901 and for the Strain-com Arr model [4] is 0.2812.

Since the modified Z–A model considers physical phenomenon similar to dislocation slip with considering processing parameters so it can predict the hot flow behavior of pure aluminum with higher accuracy than the modified J–C model which does not consider the physical phenomenon [19].

The dislocations mobilities consist of the climb and cross-slip increases rapidly with increasing temperature and usually, thermal softening processes such as DRV and DRX occur. So, considering dislocation motion with phenomenological processing parameters is very important for developing a constitutive model to predict hot flow behavior accurately [24].

4. CONCLUSIONS

The hot deformation behavior of AA1070 aluminum was investigated using hot compression tests in a wide range of T (623–773 K) and $\dot{\epsilon}$ (0.005–0.5 s⁻¹) and modified J–C and modified Z–A constitutive equations were developed to estimate the flow behavior of AA1070 at elevated temperature. Based on this study, the following are the conclusions:

- The effects of $\dot{\epsilon}$ and T on the flow behavior of AA1070 aluminum are significant at elevated temperatures as the flow stress increases with increasing $\dot{\epsilon}$ and decreasing T .
- The constitutive equations based on modified J–C and modified Z–A models have been established successfully. The developed models can predict the hot flow behavior of pure aluminum with proper accuracy.
- It is computed that the AARE value and mean RE from the modified J–C model are 9.085 and 1.662%, respectively and the corresponding R value is 0.9759.
- It is computed that the AARE value and mean RE from the modified Z–A model are 7.901 and 0.784%, respectively and the corresponding R value is 0.976.

REFERENCES

1. G. E. Totten and D. S. MacKenzie, *Handbook of Aluminum*, Vol. 1: *Physical Metallurgy and Processes* (CRC Press, Boca Raton, FL, 2004).
2. R. K. Roy and S. Das, “New combination of polishing and etching technique for revealing grain structure of an annealed aluminum (AA1235) alloy,” *J. Mater. Sci.* **41**, 289–292 (2006).
3. Y. C. Lin, M. S. Chen, and J. Zhong, “Prediction of 42CrMo steel flow stress at high temperature and strain rate,” *Mech. Res. Commun.* **35**, 142–150 (2008).
4. H. R. Rezaei Ashtiani, M. H. Parsa, and H. Bisadi, “Constitutive equations for elevated temperature flow behavior of commercial purity aluminum,” *Mater. Sci. Eng., A* **545**, 61–67 (2012).
5. Y. C. Lin and X. M. Chen, “A critical review of experimental results and constitutive descriptions for metals and alloys in hot working,” *Mater. Des.* **32**, 1733–1759 (2011).
6. S. Liu, Q. Pan, H. Li, Z. Huang, K. Li, X. He, et al., “Characterization of hot deformation behavior and constitutive modeling of Al–Mg–Si–Mn–Cr alloy,” *J. Mater. Sci.* **54** (5), 4366–4383 (2019).
7. H. J. McQueen and N. D. Ryan, “Constitutive analysis in hot working. *Mater. Sci. Eng., A* **322** (1–2), 43–63 (2002).
8. G. R. Johnson and W. H. Cook, “A constitutive model and data for metals subjected to large strains, high strain rates and high temperatures,” in *Proceedings of the 7th International Symp. of Ballistics* (Hague, 1983), pp. 541–547.
9. Y. Q. Cheng, H. Zhang, Z. H. Chen, and K. F. Xian, “Flow stress equation of AZ31 magnesium alloy sheet during warm tensile deformation,” *J. Mater. Process. Technol.* **208** (1–3), 29–34 (2008).
10. F. A. Slooff, J. Zhou, J. Duszczak, and L. Katgerman, “Constitutive analysis of wrought magnesium alloy Mg–Al4–Zn1,” *Scr. Mater.* **57** (8), 759–762 (2007).
11. H. R. Rezaei Ashtiani, M. H. Parsa, and H. Bisadi, “Effects of initial grain size on hot deformation behavior of commercial pure aluminum,” *Mater. Des.* **42**, 478–485 (2012).
12. J. Cai, K. Wang, P. Zhai, F. Li, and J. Yang, “A modified Johnson–Cook constitutive equation to predict hot deformation behavior of Ti–6Al–4V alloy,” *J. Mater. Eng. Perform.* **24** (1), 32–44 (2015).
13. K. Li, Q. Pan, R. Li, S. Liu, Z. Huang, and X. He, “Constitutive modeling of the hot deformation behavior in 6082 aluminum alloy,” *J. Mater. Eng. Perform.* **28** (2), 981–994 (2019).
14. F. J. Zerilli and R. W. Armstrong, “Dislocation-mechanics-based constitutive relations for material dynamics calculations,” *J. Appl. Phys.* **61** (5), 1816–1825 (1987).
15. H. Zhang, W. Wen, H. Cui, and Y. Xu, “A modified Zerilli–Armstrong model for alloy IC10 over a wide range of temperatures and strain rates,” *Mater. Sci. Eng., A* **527** (1–2), 328–333 (2009).
16. A. Venkata Ramana, I. Balasundar, M. J. Davidson, R. Balamuralikrishnan, and T. Raghu, “Constitutive modeling of a new high-strength low-alloy steel using modified Zerilli–Armstrong and Arrhenius model,” *Trans. Indian Inst. Met.* **72** (10), 2869–2876 (2019).
17. H. Ahmadi, H. R. Rezaei Ashtiani, and M. Heidari, “A comparative study of phenomenological, physically-based and artificial neural network models to predict the Hot flow behavior of API 5CT-L80 steel,” *Mater. Today: Commun.* **25**, 101528 (2020).
18. H. Sun, Y. Zhang, A. A. Volinsky, B. Wang, B. Tian, K. Song, et al., “Effects of Ag addition on hot deformation behavior of Cu–Ni–Si alloys,” *Adv. Eng. Mater.* **19** (3), 1600607 (2017).

19. A. Rudra, S. Das, and R. Dasgupta, "Constitutive modeling for hot deformation behavior of Al-5083 + SiC composite," *J. Mater. Eng. Perform.* **28** (1), 87–99 (2019).
20. D. Samantaray, S. Mandal, C. Phaniraj, and A. K. Bhaduri, "Flow behavior and microstructural evolution during hot deformation of AISI type 316 L(N) austenitic stainless steel," *Mater. Sci. Eng., A* **528** (29–30), 8565–8572 (2011).
21. Y. Han, G. Qiao, J. Sun, and D. Zou, "A comparative study on constitutive relationship of as-cast 904L austenitic stainless steel during hot deformation based on Arrhenius-type and artificial neural network models," *Comput. Mater. Sci.* **67**, 93–103 (2013). <https://www.sciencedirect.com/science/article/pii/S0927025612004405>. Cited September 24, 2019.
22. Y. C. Lin, X. M. Chen, and G. Liu, "A modified Johnson–Cook model for tensile behaviors of typical high-strength alloy steel," *Mater. Sci. Eng., A* **527** (26), 6980–6986 (2010).
23. D. Samantaray, S. Mandal, U. Borah, A. K. Bhaduri, and P. V. Sivaprasad, "A thermo-viscoplastic constitutive model to predict elevated-temperature flow behaviour in a titanium-modified austenitic stainless steel," *Mater. Sci. Eng., A* **526** (1–2), 1–6 (2009).
24. Y. V. R. K. Prasad, K. P. Rao, and S. Sasidhara, *Hot Working Guide: Compendium of Processing Maps* (ASM Int., Materials Park, OH, 1997).